

## Evidence for Two Energy Gaps in Superconducting $\text{Ba}_{0.6}\text{K}_{0.4}\text{Fe}_2\text{As}_2$ Single Crystals and the Breakdown of the Uemura Plot

Cong Ren,\* Zhao-Sheng Wang, Hui-Qian Luo, Huan Yang, Lei Shan, and Hai-Hu Wen†

National Laboratory for Superconductivity, Institute of Physics and Beijing National Laboratory for Condensed Matter Physics, Chinese Academy of Sciences, P.O. Box 603, Beijing 100190, China

(Received 11 August 2008; published 19 December 2008)

We report a detailed investigation on the lower critical field  $H_{c1}$  of the superconducting  $\text{Ba}_{0.6}\text{K}_{0.4}\text{Fe}_2\text{As}_2$  (122) single crystals. A pronounced kink is observed on the  $H_{c1}(T)$  curve, which is attributed to the existence of two superconducting gaps. By fitting the data  $H_{c1}(T)$  to the two-gap BCS model in the full temperature region, a small gap of  $\Delta_a(0) = 2.0 \pm 0.3$  meV and a large gap of  $\Delta_b(0) = 8.9 \pm 0.4$  meV are obtained. The in-plane penetration depth  $\lambda_{ab}(0)$  is estimated to be 105 nm corresponding to a rather large superfluid density, which points to the breakdown of the Uemura plot in 122 superconductors.

DOI: 10.1103/PhysRevLett.101.257006

PACS numbers: 74.20.Rp, 74.25.Ha, 74.70.Dd

One of the crucial issues in understanding the superconducting mechanism in recently discovered FeAs-based layered superconductors [1,2] is the pairing symmetry of the superconducting gap and the nature of the low energy excitations. For  $\text{LnFeAsO}_{1-x}\text{F}_x$  (1111) superconductors with  $x = 0.04\text{--}0.2$  and  $\text{Ln} = \text{La, Ce, Nd, Sm}$ , reports on pairing symmetry are divided into two categories: those favoring a gap with [3,4] or without [5,6] nodes. In other regards, many experimental results indicate a two-gap nature [7–11]. From the band structure point of view, the multiband model has been strengthened with pairing interactions originating from the intraband antiferromagnetic coupling plus an effective interband antiferromagnetic interaction [12,13]. However, because most of the current experiments were performed on polycrystalline samples, the experimental results within the context of pairing symmetry have not yet reached a consensus.

The emergence of  $(\text{Ba, Sr})_{1-x}\text{K}_x\text{Fe}_2\text{As}_2$  (122) [14,15] hole-doped superconductors with transition temperature  $T_c$  up to 38 K has enriched the research in this area. Although stoichiometric (undoped)  $\text{BaFe}_2\text{As}_2$  shares the same feature with undoped  $\text{LnFeAsO}$  of a spin-density-wave type magnetic order and a structural transition at similar temperatures [16], however, there are also some significant differences between the properties of 1111 and 122 superconductors. Most notable is the fact that 1111 superconductors seem to have a very low charge carrier density [2] and hence a low superfluid density [4,17]. This may give explanation to the fact that the Uemura plot is satisfied in the 1111 systems [17]. According to Uemura *et al.* [18], in superconductors with low superfluid density ( $\rho_s$ ),  $T_c$  scales linearly with  $\rho_s \propto \lambda_{ab}^{-2}(0)$ . However, it is found that the charge carrier density in 122 is an order of magnitude larger than those in 1111 systems [14,19]. Thus it is very interesting to know whether the Uemura plot is still satisfied in 122 superconductors.

Lower critical field ( $H_{c1}$ ), or equivalently, magnetic penetration depth ( $\lambda$ ) is a fundamental probe of the nature of the pairing symmetry, or/and multigap of unconven-

tional superconductors. In this Letter we present the first detailed magnetic penetration measurements of superconducting  $\text{Ba}_{0.6}\text{K}_{0.4}\text{Fe}_2\text{As}_2$  single crystals. The local magnetization measurements allow a precise determination of  $H_{c1}$ . We found the presence of a possible full gap feature together with two gaps in  $\text{Ba}_{0.6}\text{K}_{0.4}\text{Fe}_2\text{As}_2$  superconductors. Meanwhile, the absolute value of  $H_{c1}(0)$  determined from this work place the samples far away from the Uemura plot.

Crystals of  $\text{Ba}_{0.6}\text{K}_{0.4}\text{Fe}_2\text{As}_2$  were grown by the FeAs flux method [19]. Our crystals were characterized by resistivity measurements with  $T_c = 36.2$  K and a transition width of  $\Delta T_c = 0.45$  K (10%–90% of normal state resistivity) [19], as displayed in the left inset of Fig. 1(a). A single crystal (sample No. 1) was selected from the cleaved as-grown bulk under optical microscope. The sample has dimensions of 110  $\mu\text{m}$  in diameter and 40  $\mu\text{m}$  in thickness, as shown in the right inset of Fig. 1(a). The crystal structure was examined by x-ray diffraction, and only (00 $l$ ) peaks were observed with the full-width-at-half-maximum around  $0.1^\circ$ , as shown in the main panel of Fig. 1(a), which indicates good crystallization of our samples.

The local magnetization measurement was performed on two crystals using a two-dimensional electron gas based micro Hall sensor with an active area of  $10 \times 10 \mu\text{m}^2$ . The Hall sensor was characterized without sample attachment at different temperatures. In our experiment, we used a small field sweep rate of 30 Oe/min to measure the isothermal magnetization  $M(H)$  curves in both decreasing ( $M_{\text{dec}}$ ) and increasing ( $M_{\text{inc}}$ ) the fields to minimize the complex effects of the character of the field penetration in a layered structure [20]. The pinning property has been checked by measuring the magnetization hysteresis loops. The result is shown in the inset of Fig. 1(b). The  $M(H)$  curve shows a symmetric feature at  $T = 32.1$  K, indicative of the dominance of bulk pinning and the absence of the Bean-Livingston surface barrier for vortex entry. A second crystal (sample No. 2) with dimensions of  $210 \times 150 \times 50 \mu\text{m}^3$  was also measured by Hall sensor and vibrating

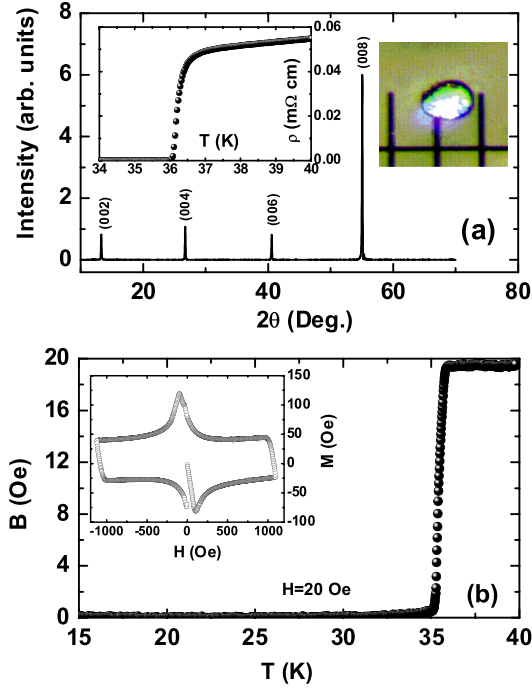


FIG. 1 (color online). (a) X-ray diffraction pattern of the  $\text{Ba}_{0.6}\text{K}_{0.4}\text{Fe}_2\text{As}_2$  crystal. The right inset shows the sample (No. 1) under the optical microscope. The scale underneath with  $100 \mu\text{m}/\text{grid}$  is used to display the size of the sample. The left inset shows the resistive transition on one crystal cut from the same piece. (b) The induction  $B$  by Hall probe as a function of  $T$  measured in zero-field-cooled mode. Inset: A typical magnetization hysteresis loop measured at  $32.1 \text{ K}$  by the Hall sensor.

sample magnetometry, and both measurements showed essentially identical behavior except for the different demagnetization effect.

The quality of the crystal and the accuracy of the local magnetization measurement are demonstrated in Fig. 1(b), in which the induction  $B = H + 4\pi M$  sensed by the Hall probe is plotted as a function of  $T$  under a bias field  $H = 20 \text{ Oe}$ . The superconducting transition can be detected as the induction jump at  $T_c = 35.8 \text{ K}$  with a width of  $\Delta T_c = 0.5 \text{ K}$ , which shows the high quality of the crystal. As shown in raw data of  $B(T)$ , at low temperatures,  $B$  is close to 0, implying a full Meissner shielding effect:  $4\pi M \approx -H$ . Thus the achievement of the full Meissner shielding effect in our measurement provides a reliable way to determine the value of  $H_{c1}$ .

Shown in Fig. 2(a) are the typical isothermal  $M(H)$  curves by taking  $M_{\text{dec}}$  and  $M_{\text{inc}}$  at  $T = 17.1 \text{ K}$ , respectively. It can be seen that, at low  $H$ , the  $M_{\text{dec}}$  and  $M_{\text{inc}}$  are fully reversible, showing a common linear dependence of the magnetization on field as displayed in the bottom-left inset of Fig. 2(a). At high  $H$ , a deviation from the linear dependence occurs at  $H = H_{c1}$  for both  $M_{\text{dec}}$  and  $M_{\text{inc}}$  curves. To distinguish these deviations, we fit more than 50 data points between 10 and 30 Oe by a linear relation to account for the common linear dependence of  $M(H)$ .

These fitted linear lines describe the Meissner shielding effects (“Meissner line”) at low fields, as evidenced quantitatively in Fig. 2(a) in which the slope of the fitted lines are  $-0.98$ , very close to  $-1$ . Thus the deviation of  $M(H)$  from the linear Meissner shielding is an indication of the first penetration field  $H_{c1}$ . An alternative way to determine the value of  $H_{c1}$  from these reversible isothermal  $M(H)$  curves is to subtract the Meissner line from both  $M_{\text{dec}}(H)$  and  $M_{\text{inc}}(H)$  curves, as illustrated in the upper-right inset of Fig. 2(a). The threshold field of nonzero magnetization happens to be the divergence of the increasing and decreasing  $M(H)$  curves. It is noted that the values of  $H_{c1}$  with this criterion were determined in both increasing and decreasing field, so they are the true thermodynamic values and are not altered by the surface barrier [20]. For a strict treatment, we determined the value of  $H_{c1}$  by examining the point of departure from the Meissner line on the initial slope of the  $M(H)$  curve. In the inset of Fig. 2(b) we show how to determine  $H_{c1}$  by using a criterion of  $B = \Delta M = 0.5 \text{ Oe}$  at different temperatures. For a quantum flux  $\phi_0 = 20.7 \text{ Oe} \mu\text{m}^2$ ,  $\Delta M = 0.5 \text{ Oe}$  is equivalent to about  $2\text{--}3 \phi_0$

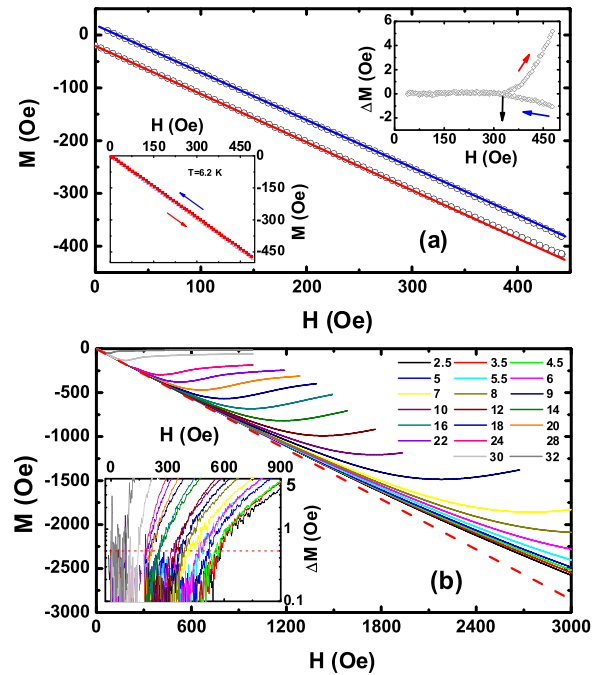


FIG. 2 (color online). (a) A typical magnetization hysteresis loop (symbols), the solid lines are the linear fitting curves using the low field data (Meissner line). The increasing and decreasing branches are shifted downward and upward, respectively, for clarity. The same case is shown in the bottom-left inset when the maximum field is less than  $H_{c1}$ . The upper-right inset shows the magnetization data subtracted by the Meissner line. The arrows indicate the direction of sweeping fields and the determination of  $H_{c1}$ . (b) The initial part of the magnetization curves  $M(H)$  of sample No. 2 at various temperatures. The dashed line gives the Meissner linear approach. Inset: The same magnetization data in field subtracted by the Meissner line. The dashed line in the inset sets up a criterion of  $0.5 \text{ Oe}$ .

penetrating into the  $(10 \times 10) \mu\text{m}^2$  sensing area, which is the limit of our Hall probe technique. The  $H_{c1}$  values determined in this way are about 4% larger than those estimated from the point where the reversible magnetization deviates from linearity, and we did not observe any significant difference in the  $T$  dependence of  $H_{c1}$  deduced from either of the two criterion.

Shown in Fig. 3(a) and 3(b) are the obtained  $H_{c1}$  plotted as a function of  $T$  for crystals No. 1 and 2, respectively. At  $T < 4 \sim 5$  K,  $H_{c1}(T)$  is weakly  $T$  dependent and seems to show a tendency towards saturation at lower  $T$  (in the limited temperature range). As illustrated in the insets of Fig. 3(a) and 3(b), the saturated  $H_{c1}$  reach 695 Oe for sample No. 1 and 590 Oe for sample No. 2. This tendency of  $H_{c1}(T)$  reflects a possible fully gapped nature of superconducting state at low  $T$  for  $\text{Ba}_{0.6}\text{K}_{0.4}\text{Fe}_2\text{As}_2$  superconductors. With these data, we could not rule out the possibility of a small gap with nodes in the dirty limit with  $\rho_s(T)$  decaying with  $T^2$ , as in the cuprate superconductors, which will lead to even larger  $\rho_s(0)$  and  $H_{c1}(0)$  as one would expect in the clean limit.

A pronounced *kink* can be easily observed in  $H_{c1}(T)$  curves at  $T \sim 15$  K for both samples. Obviously, the occurrence of the kink in  $H_{c1}(T)$  cannot be explained by the model with an *s*-wave or *d*-wave *single gap*. On the other

hand, this kinky structure in  $H_{c1}(T)$  resembles that of the related superfluid density of the two-band superconductor  $\text{MgB}_2$  [21], in which a positive curvature was observed and explained by the multiband theory [22]. In addition, recent angle-resolved photoemission spectroscopy (ARPES) revealed a two-gap nature in a similar  $\text{Ba}_{0.6}\text{K}_{0.4}\text{Fe}_2\text{As}_2$  crystal [23]. Thus our observation of a kink in  $H_{c1}(T)$  strongly suggests the existence of multiple gaps in  $\text{Ba}_{0.6}\text{K}_{0.4}\text{Fe}_2\text{As}_2$  superconductors, which is consistent with that predicted in electronic band structure calculations [24].

For our crystals, assuming  $\lambda_{ab}(0) \sim 100\text{--}200$  nm [25], the coherence length  $\xi_{ab}^c(0)$  was estimated to be 2–2.5 nm from an extremely high upper critical field  $H_{c2}$  [ $\mu_0 H_{c2}^{\parallel c}(0) = \phi_0/2\pi\xi_{ab}^2(0)$ ] [19,26], and the mean free path (determined from the resistivity and the Hall effect data at 38 K) is  $\sim 15$  nm, our samples are therefore in the moderately clean, local limit. In this case the local London model is valid to describe the data. For a single gap superconductor,  $H_{c1}$  relates the normalized superfluid density as:  $\tilde{\rho}_s(T) \equiv \lambda_{ab}^2(0)/\lambda_{ab}^2(T) = H_{c1}(T)/H_{c1}(0)$ , and  $\tilde{\rho}_s(T)$  is given by [27,28]

$$\tilde{\rho}_s(T) = 1 + 2 \int_0^\infty \frac{df(E)}{dE} \frac{E}{\sqrt{E^2 - \Delta(T)^2}} dE \quad (1)$$

with  $f$  the Fermi function. Here the total energy is  $E = \sqrt{\epsilon^2 + \Delta^2}$ , and  $\epsilon$  is the single-particle energy measured from the Fermi surface. We should note that the equation above is based on the assumption of an isotropic Fermi velocity and gap, which may be validated by the very small anisotropy (about 2) determined from the transport measurements [29]. It is assumed that the gap  $\Delta$  on each Fermi surface follows the weak-coupling BCS temperature dependence. For a superconductor with two gaps, the normalized superfluid density may be written as:  $\tilde{\rho}_s = x\tilde{\rho}_s^a + (1-x)\tilde{\rho}_s^b$ , where  $x$  is the fraction of superfluid density  $\tilde{\rho}_s^a$  associated with the small gap  $\Delta_a$ . The results of the calculations and  $H_{c1}$  of sample No. 1 and 2 are shown by the red solid lines in Fig. 3(a) and 3(b), respectively. Fitting the data to the equations above (with two *s*-wave gaps) yields:  $\Delta_a = 1.6 \pm 0.3$  meV,  $\Delta_b = 9.1 \pm 0.3$  meV and  $x = 0.72$  for sample No. 1, and  $\Delta_a = 2.2 \pm 0.2$  meV,  $\Delta_b = 8.8 \pm 0.3$  meV and  $x = 0.70$  for sample No. 2. We also tried to fit our data with a single *s*-wave gap which is anisotropic, having an in-plane angle dependence,  $\Delta(T, \varphi) = \Delta(T) \times (1 + \alpha \cos^2 \varphi)/(1 + \alpha)$ , where  $\alpha$  is a fitting parameter which controls the anisotropy. The overall fitting in wide temperature regime is in serious disagreement with our data. Thus the possibility of a single anisotropic gap seems unlikely when considering the almost symmetric circlelike Fermi surfaces in the present system.

The gaps obtained from our  $H_{c1}(T)$  measurements are clearly smaller than those determined from the ARPES measurements [23]. This discrepancy may be induced by the different ways and different criterions in determining the gaps, this should be checked by future experiments. It is interesting to note that the large gap accounts for only 30%

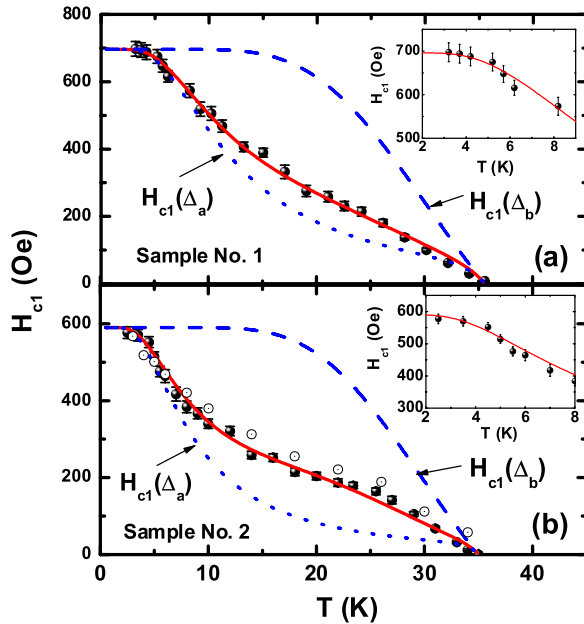


FIG. 3 (color online). The extracted  $H_{c1}$  as a function of  $T$  for sample No. 1 (a) and No. 2 (b) (full circles with error bars). The open dotted circles in (b) represent the  $H_{c1}$  determined from the vibrating sample magnetometry measurements taken into account of the demagnetization effect. The solid lines are the fitting curves using the two-gap model. The contributions of the small gap [ $H_{c1}(\Delta_a)$ ] and the large gap [ $H_{c1}(\Delta_b)$ ] in the model are also shown by the dotted and dashed lines, respectively. The two insets in (a) and (b) show the enlarged views of the data  $H_{c1}(T)$  in low temperature region together with the theoretical fitting curves (solid lines).

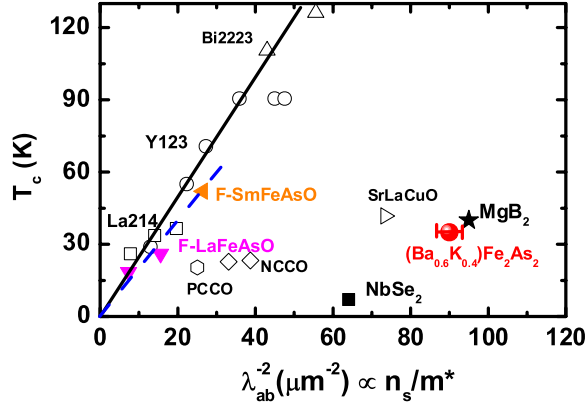


FIG. 4 (color online). The correlations between  $T_c$  and the superfluid density  $n_s/m^*$ . Points for the cuprates are taken from Ref. [17]. The full triangles show the data for F-LaFeAsO (Ref. [3,17]) and F-SmFeAsO (Ref. [10] and our work). The data of MgB<sub>2</sub> and NbSe<sub>2</sub> are taken from Ref. [21,30], respectively.

of the total superfluid density. We must stress that although a small gap with nodes (in the dirty limit) cannot be excluded from our low temperature data, this will not lead to a significant change to the general fitting results obtained here.

Another important result of our experiment, the absolute value of  $\lambda_{ab}(0)$  is *independently* deduced from the measured  $H_{c1}(0)$ . In principle, we evaluate the penetration depth  $\lambda_{ab}(0)$  using the expression:  $H_{c1}^{\parallel c} = (\phi_0/4\pi\lambda_{ab}^2) \times \ln\kappa$ , where  $\kappa = \lambda/\xi$  is the Ginzburg-Landau parameter (here we assume that  $\kappa$  is  $T$  independent). Using  $H_{c1}^{\parallel c}(0) = 695$  Oe and  $\kappa = 80$ , we obtain  $\lambda_{ab}(0) \approx 105$  nm for sample No. 1 and 115 nm for sample No. 2. The value of  $\lambda_{ab}^{-2}(0)$ , or equivalently the condensed carrier density  $n_s/m^*$  (superconducting carrier density/effective mass), allows us to check whether the well-known scaling behavior between  $n_s/m^*$  and  $T_c$  still works for the present system. In Fig. 4 we present our results together with many others, including the 1111 system, cuprates, MgB<sub>2</sub>, and NbSe<sub>2</sub> [30]. It is remarkable that Ba<sub>0.6</sub>K<sub>0.4</sub>Fe<sub>2</sub>As<sub>2</sub> resides far away from the Uemura plot, which is contrasted by the case of the 1111 system which is quite close to the Uemura plot. This discrepancy between 122 and 1111 implies a very essential difference between the physics in the two systems and warrants further investigation.

To summarize, we conduct magnetization measurements on Ba<sub>0.6</sub>K<sub>0.4</sub>Fe<sub>2</sub>As<sub>2</sub> single crystals, and the lower critical field  $H_{c1}(T)$  is reliably extracted. It is found that  $H_{c1}$  exhibits a pronounced kink at  $T \sim 15$  K, which indicates a multigap nature. By using the two-gap weak-coupling BCS model to fit the data, we obtained a small gap of  $\Delta_a(0) \approx 2.0 \pm 0.3$  meV and a large gap of  $\Delta_b(0) \approx 8.9 \pm 0.4$  meV. An estimate of the in-plane penetration depth gives  $\lambda_{ab}(0) \approx 105$  nm, which points to the breakdown of the Uemura relation for the optimally doped Ba<sub>0.6</sub>K<sub>0.4</sub>Fe<sub>2</sub>As<sub>2</sub> superconductors.

The authors are grateful to Junren Shi, Tao Xiang and Jan Zaanan for helpful discussions, and Wen-Xin Wang and Hong Chen for providing us the GaAs/AlGaAs substrates. This work is supported by the Natural Science Foundation of China, 973 Projects No. 2006CB60100, No. 2006CB921107, No. 2006CB921802), and Chinese Academy of Sciences (Project ITSNEM).

\*cong\_ren@aphy.iphy.ac.cn

†hhwen@aphy.iphy.ac.cn

- [1] Y. Kamihara *et al.*, J. Am. Chem. Soc. **130**, 3296 (2008).
- [2] G.F. Chen *et al.*, Phys. Rev. Lett. **100**, 247002 (2008); X.Y. Zhu *et al.*, Supercond. Sci. Technol. **21**, 105001 (2008); X.H. Chen *et al.*, Nature (London) **453**, 761 (2008); Z.A. Ren *et al.*, Chin. Phys. Lett. **25**, 2215 (2008).
- [3] G. Mu *et al.*, Chin. Phys. Lett. **25**, 2221 (2008); L. Shan *et al.*, Europhys. Lett. **83**, 57004 (2008); C. Ren *et al.*, arXiv:0804.1726.
- [4] Y. Nakai *et al.*, arXiv:0804.4765; M.C. Boyer *et al.*, arXiv:0806.4400.
- [5] T.Y. Chen *et al.*, Nature (London) **453**, 1224 (2008).
- [6] K. Hashimoto *et al.*, arXiv:0806.3149; C. Martin *et al.*, arXiv:0807.0876.
- [7] F. Hunte *et al.*, Nature (London) **453**, 903 (2008).
- [8] Y.L. Wang *et al.*, arXiv:0806.1986.
- [9] K. Matano *et al.*, Europhys. Lett. **83**, 57001 (2008).
- [10] A.J. Drew *et al.*, Phys. Rev. Lett. **101**, 097010 (2008); L. Malone *et al.*, arXiv:0806.3908.
- [11] I. Felner *et al.*, arXiv:0805.2794.
- [12] Q. Han, Y. Chen, and Z.D. Wang, Europhys. Lett. **82**, 37007 (2008).
- [13] V. Cvetkovic and Z. Tesanovic, arXiv:0804.4678.
- [14] M. Rotter, M. Tegel, and D. Johrendt, Phys. Rev. Lett. **101**, 107006 (2008).
- [15] K. Sasmal *et al.*, Phys. Rev. Lett. **101**, 107007 (2008).
- [16] M. Rotter *et al.*, Phys. Rev. B **78**, 020503 (2008); Q. Huang *et al.*, arXiv:0806.2776 [Phys. Rev. Lett. (to be published)].
- [17] H. Luetkens *et al.*, Phys. Rev. Lett. **101**, 097009 (2008); J.P. Carlo *et al.*, arXiv:0805.2186.
- [18] Y.J. Uemura *et al.*, Phys. Rev. Lett. **66**, 2665 (1991).
- [19] H.Q. Luo *et al.*, Supercond. Sci. Technol. **21**, 125014 (2008).
- [20] R. Liang, D.A. Bonn, W.N. Hardy, and D. Broun, Phys. Rev. Lett. **94**, 117001 (2005).
- [21] F. Manzano *et al.*, Phys. Rev. Lett. **88**, 047002 (2002).
- [22] A.A. Golubov *et al.*, Phys. Rev. B **66**, 054524 (2002).
- [23] H. Ding *et al.*, Europhys. Lett. **83**, 47001 (2008); L. Zhao *et al.*, Chin. Phys. Lett. **25**, 4402 (2008).
- [24] F. Wang *et al.*, arXiv:0807.0498.
- [25] G. Li *et al.*, Phys. Rev. Lett. **101**, 107004 (2008).
- [26] M. Altarawneh *et al.*, arXiv:0807.4488.
- [27] A. Carrington and F. Manzano, Physica C (Amsterdam) **385**, 205 (2003).
- [28] H.G. Luo and T. Xiang, Phys. Rev. Lett. **94**, 027001 (2005).
- [29] Z.S. Wang *et al.*, Phys. Rev. B **78**, 140501 (2008).
- [30] J.D. Fletcher *et al.*, Phys. Rev. Lett. **98**, 057003 (2007).